Research Article | Vol. 29, No. 4 / 15 February 2021 / Optics Express 5397
Optics EXPRESS

High-efficient coupler for thin-film lithium niobate waveguide devices

CHANGRAN HU,[1] AN PAN,[1] TINGAN LI,[1] XUANHAO WANG,[1] YUHENG LIU,[1] SHIQI TAO,[1] CHENG ZENG,[1,2] AND JINSONG XIA[1,3]

[1] *Wuhan National Laboratory for Optoelectronics, Huazhong University of Science and Technology, Wuhan 430074, China*
[2] *zengchengwuli@hust.edu.cn*
[3] *jsxia@hust.edu.cn*

Abstract: Lithium niobate (LN) devices have been widely used in optical communication and nonlinear optics due to its attractive optical properties. The emergence of the thin-film lithium niobate on insulator (LNOI) improves performances of LN-based devices greatly. However, a high-efficient fiber-chip optical coupler is still necessary for the LNOI-based devices for practical applications. In this paper, we demonstrate a highly efficient and polarization-independent edge coupler based on LNOI. The coupler, fabricated by a standard semiconductor process, shows a low fiber-chip coupling loss of 0.54 dB/0.59 dB per facet at 1550 nm for TE/TM light, respectively, when coupled with an ultra-high numerical aperture fiber (UHNAF) of which the mode field diameter is about 3.2 μm. The coupling loss is lower than 1dB/facet for both TE and TM light in the wavelength range of 1527 nm to 1630 nm. A relatively large tolerance for optical misalignment is also proved, due to the coupler's large mode spot size up to 3.2 μm. The coupler shows a promising stability in high optical power and temperature variation.

1. Introduction

Over the last two decades, significant progress in the photonic integrated circuits (PICs) based on Si have been made [1,2]. They are crucial for the performance of various optical transmission systems. Recently, the LNOI attracts more and more intention from both industry and research institutions and is considered as a promising candidate for new-generation PICs platform due to its potential for ultra-high-speed application. Recently, various devices based on LNOI have been reported and shown outstanding performance, such as low-loss optical waveguide, high-Q ring resonator [3], tunable filter [4], high speed EO modulator [5], optical frequency comb [6], second harmonic generator [7], wavelength convertor [8], spectrometer [9], etc. However, a highly efficient, polarization independent and wide-band fiber-chip optical coupler is still absent, which is critical essential for these devices to be used in practical applications.

Directly-coupling is widely used in traditional bulk lithium niobate platform [10]. But the huge difference between mode-field-diameter (MFD) of standard-single-mode-fiber (SSMF, ~10μm) and integrated waveguide on LNOI(<1μm) leads to a great optical loss in this configuration. Researchers try to make use of the lensed taper fiber to improve the coupling efficiency, but the experimental result is still not good enough [5,8,9]. To realize fiber-chip coupling, various optical couplers, such as grating coupler [11], prism coupler [12], horizontal edge coupler [13–23] can be used. The grating coupler is limited to its bandwidth and polarization-dependence. As to prism coupler, a stable mechanical pressure is required to hold the prism in right place [24]. Evanescent coupling is another intuitive scheme utilizing the energy transfer between two closed optical waveguides [25–27], but usually at the cost of the special tapered fibers and uncovered parts of devices, as well as the difficulty in optical packaging. Researchers have also proposed novel optical couplers made by polymer utilizing 3D direct laser writing (DLW), which is based on 3D-printed freeform micro-lenses that are connected to on-chip waveguides by photonic wire

#416492 https://doi.org/10.1364/OE.416492
Journal © 2021 Received 2 Dec 2020; revised 20 Jan 2021; accepted 26 Jan 2021; published 4 Feb 2021

Optics EXPRESS

bonds (PWB) [28,29]. But the mechanical and thermal Stabilities for the suspended polymer structures are still needed to be proved. Comparing with these coupling schemes mentioned above, horizontal edge couplers [20] better meet the requirements of practical applications due to its advantages of high coupling efficiency, wide band, polarization independence, as well as stability and ease of packaging.

Recently, various kinds of edge couplers based on LNOI have been reported. For example, Chemical-mechanical polishing (CMP) is utilized to fabricate waveguide covered with tantalum oxide [13], but it is hardly compatible with general ridge waveguide. Mode matching between ridge waveguide and lensed taper fiber through a single ridge taper [14] is also demonstrated, but the coupling loss is still relatively high. To solve these problems, bilayer taper couplers have been proposed to improve the performance [15]. But the mode field distribution of the coupler controlled only by the geometry of the taper's tip is different with that of fiber. So, it is difficult to further improve the coupling efficiency in that configuration. Recently, researchers reported an edge coupler consisting of a bilayer taper and a cladding waveguide (CLDWG) which made up of polymer showing a coupling loss of 1.5dB per facet [30]. But the existence of polymer in the coupler structure can bring mechanical and thermal instability, thereby limiting its application scenarios. Besides, all the mode fields diameters of the edge couplers mentioned above is smaller than 2.5 μm [13–15, 30].

In this paper, we demonstrate a highly efficient, wide-band and polarization independent edge coupler based on LNOI fabricated by standard semiconductor process. It shows relatively large tolerance of fiber-chip misalignment and power stability. The measured UHNAF-to-chip optical coupling loss of 0.54 dB/facet (0.59 dB/facet) for TE(TM) at 1550 nm is achieved. The coupling loss is lower than 1dB/facet for both TE and TM light in the wavelength range of 1527 nm to 1630 nm. For TE light at 1550nm, the coupler's loss increases by 0.41 dB when the input power is increased to 30 dBm and an increase of 0.6 dB per facet in loss is induced by a 1-μm misalignment between the fiber end and coupler along X/Z direction. Besides, the thermal stability of the coupling by fitting and adhere the UHNAF using UV curing adhesive is also impressive. The max degradation of coupling efficient for TE light at 1550 nm is less than 0.01 dB when cycling the temperature from -45 ℃ to 75 ℃ in 2.5 hours.

2. Design and simulation

The schematic structure of the coupler is shown in Figs. 1(a) and 1(b). It consists of two parts, a bilayer LN taper to convert the mode adiabatically, and a silicon oxynitride (SiON) CLDWG. The CLDWG is used to define the shape and effective index of the mode profile at the facet of the coupler, while preventing the energy leakage into the substrate beneath the buried oxide (BOX). The refractive index of SiON is about 1.56 which is determined by the index of the UV adhesives we used. The width and height of the ridge waveguide (RWG) are designed to be 0.9 μm and 0.26 μm on a 0.24-μm-thick slab to operate in single-mode-condition. Bilayer LN taper is divided into three sections. Firstly, LN slab region narrows linearly while keeping the waveguide width unchanged. Secondly, the width of lower LN slab and width of the ridge reduce simultaneously to form the upper inversed taper. Finally, the lower slab width reduces to form the lower inversed taper. In fact, to obtained high coupling efficiency the tip width of lower inversed taper should be small enough, which is limited by the fabrication process. A cladding SiON waveguide covers the whole taper area. The chip is protected by a SiO_2 layer deposited by PECVD (Cladding SiO_2 is omitted in Fig. 1).

The coupler is designed to couple with an UHNAF with mode field diameter (MFD) of 3.2 μm. We simulated the fundamental mode of CLDWG to optimize the parameters, including the size of the CLDWG and material index. The MFD of TE0 and TM0 of CLDWG are also about 3.2 μm. The Eigenmode Expansion (EME) solver and the Finite Difference Eigenmode (FDE) solver are used to simulate the coupler. A coupling loss of 0.07 dB (0.06 dB) per facet is obtained for

Optics EXPRESS

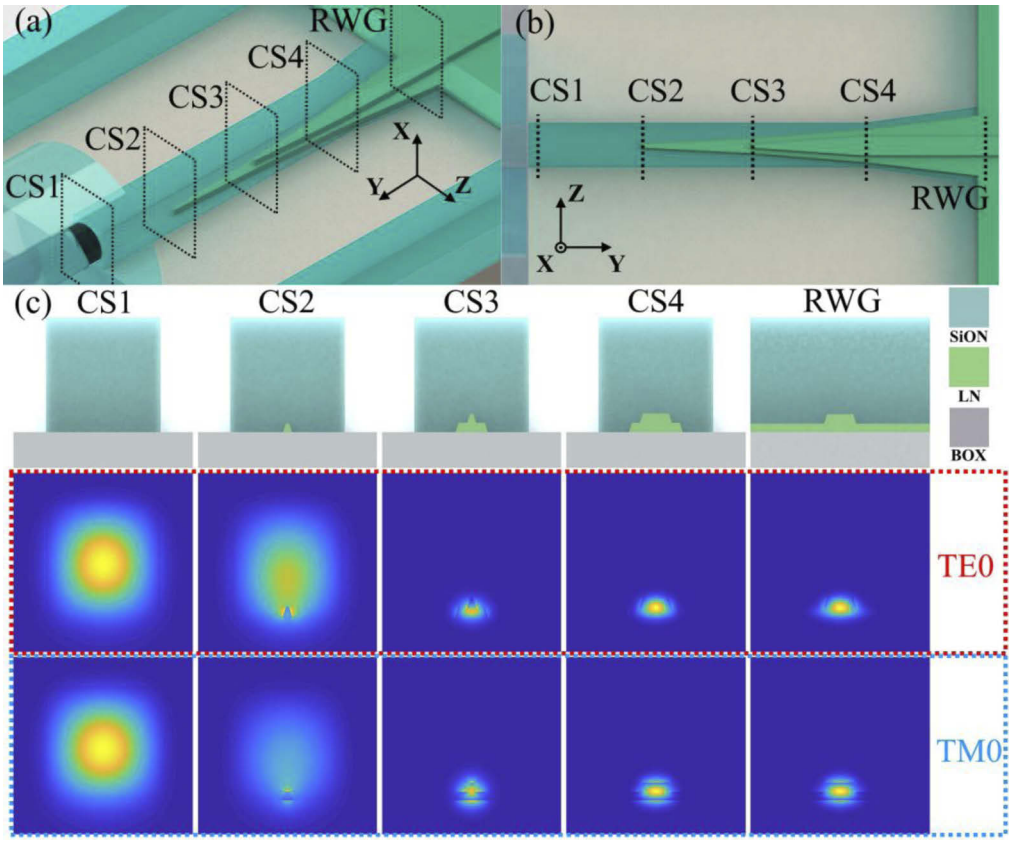

Fig. 1. (a) Schematic structure of the edge coupler. (b) Top view of the edge coupler. (c) Cross section views of the coupler and corresponding Ez and Ex distribution of fundamental TE and TM mode, respectively.

TE(TM) light in simulations after optimization. The coupling loss includes the power coupling loss at CS1 as well as the mode conversion loss from CS1 to CS5. The cross-section (CS) view and corresponding mode field distribution of at different points of the coupler are shown in Fig. 1(c). As shown in Fig. 1(c), CS1 shows the TE0/TM0 mode profiles supported by the SiON CLDWG, which are like the mode supported by the UHNAF with a 3.2-μm MFD. Therefore, the light can be coupled efficiently into the CLDWG from the UHNAF. Then, the modes are gradually "absorbed" into the lower LN taper as shown in CS2 and CS3. After that, the mode continues to transform adiabatically into the fundamental mode supported by the normal LN ridge waveguide through the upper inversed LN taper. The dimension parameters of the CLDWG and the bilayer taper are marked in Figs. 2(a) and 2(b), respectively. The CLDWG H and CLDWG W in Fig. 2(a) represent the height and the width of the CLDWG, respectively. The TL and TW in Fig. 2(b) represent the lengths and the widths of the bilayer taper, respectively. The WG W in Fig. 2(b) represents the widths of the ridge waveguide. The optimized values are listed in the Table 1. The influence of those parameters to the coupling loss is discussed in Supplement 1.

Optics EXPRESS

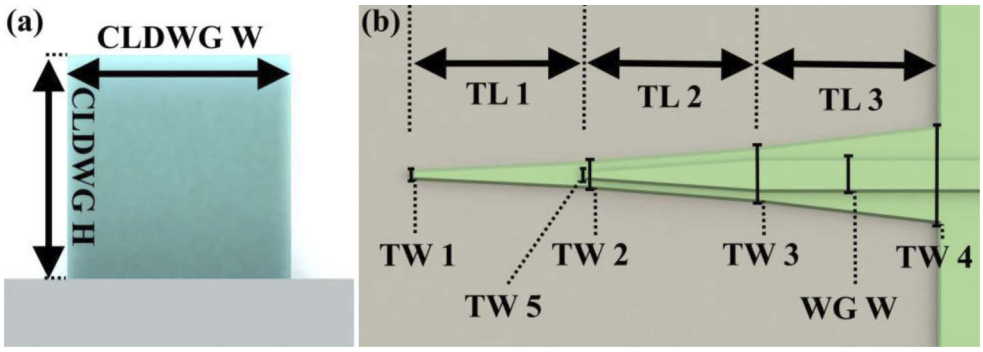

Fig. 2. (a) Dimension parameters of the CLDWG. (b) Dimension parameters of the bilayer taper.

Table 1. Optimized parameters of the coupler.

Parameter	Value	Parameter	Value	Parameter	Value
Index of SiON	1.56	TL 1	100 μm	TW 2	1.5 μm
CLDWG W	3.2 μm	TL 2	50 μm	TW 3	1.8 μm
CLDWG H	3.2 μm	TL 3	50 μm	TW 4	4 μm
WG W	0.9 μm	TW 1	0.26 μm	TW 5	0.15 μm

3. Fabrication and measurement

We fabricated the coupler on a commercially available X-cut LNOI substrate (NANOLN). The top LN thin film is 500-nm thick, and the buried oxide is 4.7-μm thick. The coupler is fabricated

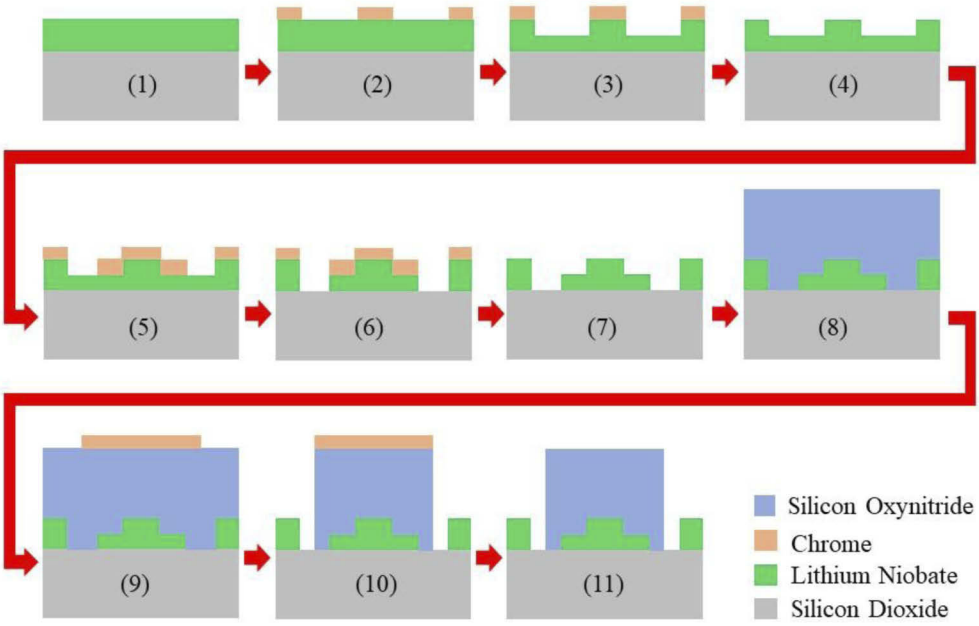

Fig. 3. Fabrication process of the coupler.

Optics EXPRESS

through the process shown as Fig. 3. First, we wash the chip by the acid and the acetone to get a clean LNOI chip as shown in step (1). Then, E-beam is used to define the waveguide and the upper taper, and the pattern is transferred to the chrome as shown in step (2). Patterning is done in step (2) to step (4). Next, the patterned chrome is used as hard mask in the ICP-RIE etching of lithium niobate in which the argon is used. Remining chrome is remove by chromium etchant. As shown in step (5) to step (7), we repeat step (2) to step (4) to make the lower taper. TW 1, namely the tip width of the lower LN inversed taper affects significantly to the coupling loss and its actual value is sensitive to the fabrication condition, as discussed in Supplement 1. To find out the optimized value, the lower LN inversed tapers with various tip widths were fabricated in this step. Then, 3.2 um thickness of silicon oxynitride is grown on the whole chip by plasma enhanced chemical vapor deposition (PECVD) in which silane, ammonia as well as nitrous oxide is used. Step (9) to step (11) show the process of the E-beam patterning of the silicon oxynitride cladding waveguide. Same as the above steps, we used ICP-RIE (sulfur hexafluoride and carbon tetrafluoride) and chrome hard mask to define the cladding waveguide. Finally, the whole chip is cladded by silicon dioxide which is omitted in Fig. 3 and the low roughness end face is made by end face polishing.

As is shown in Fig. 3, there are three times E-beam patterning in the whole fabrication process. The overlay misalignment between each E-beam lithography cannot be avoided completely, so the tolerance of the overlay misalignment along Z axis is analyzed by simulation. As is shown in Fig. 4(a), the additional loss introduced by 200 nm lateral offset of the upper taper is lower than 0.1dB. And Fig. 4(b) indicates that the additional loss introduced by 200 nm lateral offset of the CLDWG is lower than 0.004dB. Considering the overlay misalignment introduced by our E-beam equipment is almost within ±200 nm, the coupler may have a good tolerance of fabrication.

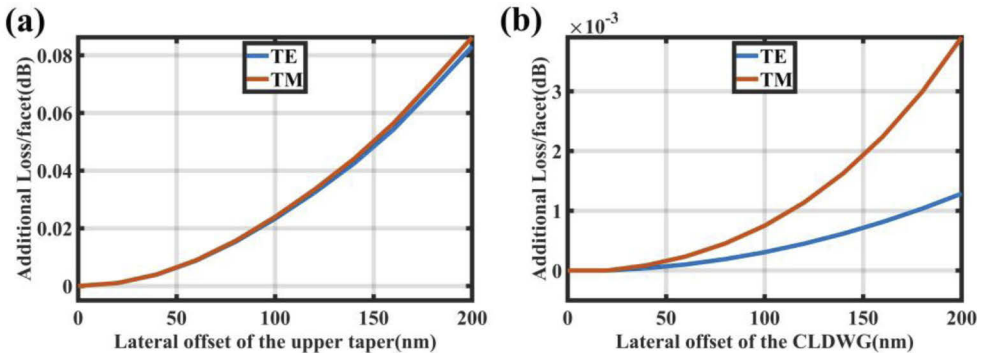

Fig. 4. (a) Dependence of additional coupling loss on lateral offset (along Z axis) of the upper taper for TE and TM polarization. (b) Dependence of additional coupling loss on lateral offset (along Z axis) of the CLDWG for TE and TM polarization.

The scanning electron microscope (SEM) images of the CLDWG and LN taper are shown in Fig. 5.

A tunable laser (Santec TLS-510) is used as the light source in the measurement of optical coupling test and the UHNFA is fused with the single mode fiber (SMF). The light from the UHNAF with a flat head was coupled into the chip after amplified by an erbium-doped fiber amplifier (EDFA) and polarized by a polarization controller (PC). Index matching oil with an index of 1.46 was used to match the index between the UHNAF and the edge coupler to reduce reflection. Passing through a LNOI ridge waveguide, the light was coupled out from the chip using the same configuration and finally detected by an optical power meter (YOKOGAWA AQ2211). The loss spectrum of the coupler is obtained by continuous scanning the wavelength from 1500 nm to 1630 nm. The configuration of the coupling test system is shown in Fig. 6.

Optics EXPRESS

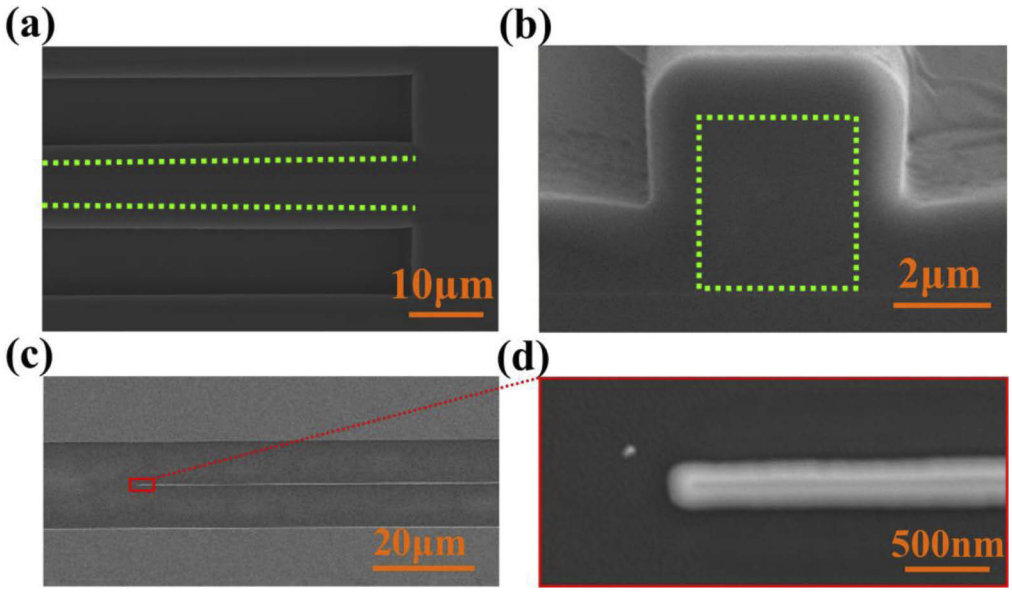

Fig. 5. (a) Scanning electron microscope image of the spot size convertor. The CLDWG is marked by the green dotted lines. (b) Scanning electron microscope image of the polished facet of the coupler. The CLDWG is marked by the green dotted lines. (c) Scanning electron microscope image of the lower inversed LN taper. (d) Scanning electron microscope image of the tip of lower inversed LN taper.

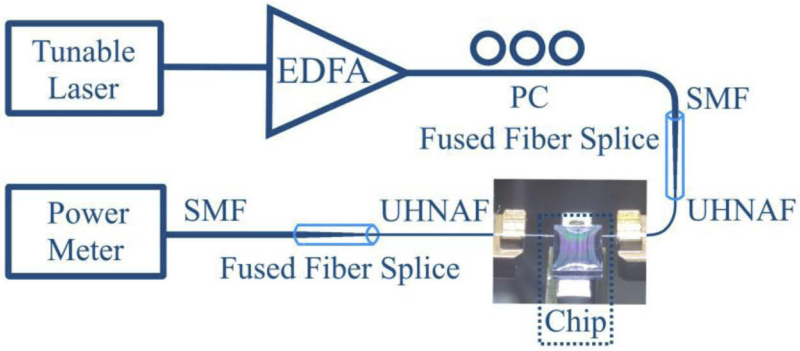

Fig. 6. The configuration of the coupling test system.

As Fig. S3 shows in Supplement 1, the propagation losses of the ridge waveguide for TE and TM fundamental mode are assessed at about 0.99dB/cm±0.11dB/cm and 1.54dB/cm±0.13dB/cm, respectively. With the loss introduced by the fused fiber splice and the LNOI ridge waveguide deducted, the measured loss spectrum of the single coupler is shown in Fig. 7(a). The coupling loss is evaluated to be 0.54 dB/facet and 0.59 dB/facet at 1550 nm for TE and TM light and the polarization extinction ratio is low than 0.05dB at 1550 nm. And the coupler shows a coupling loss lower than 1dB/facet in the whole C + L-band (1530 to 1625 nm). The loss decreases when the wavelength increases since it is equivalent to shrinking the size of the tapers' tips. An accelerating upward trend of loss is observed when the wavelength decreases. One reason is that the tip width is not small enough for the shorter wavelengths. Another possible reason is the optical absorption of plasma deposited SiON at around 1510 nm [31–33]. The widening of

Optics EXPRESS

coupler's operating wavelength might be achieved by changing the material of CLDWG, inserting a SiO_2 spacer layer between LN taper and SiON waveguide [33], and reducing the tip width further. Moreover, to get the mode spot of the coupler, the light is launched by a fiber from one end of the chip and photographed by an infrared camera at the other end, as the inset of Fig. 7(a) shows. The measured horizontal and vertical sizes of the spot are 3.12 μm and 3.07 μm, respectively. The measured spot size is smaller than the design value and it is introduced by the fabrication inaccuracy. Besides, we prove that the light transmitting from slab modes can be neglected (see Supplement 1 for more details).

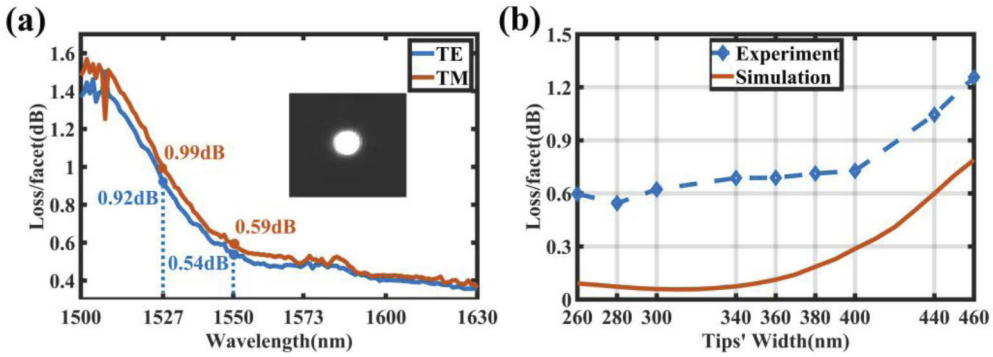

Fig. 7. (a) Coupling loss of the fabricated coupler. Inset: The fundamental TE mode spot of the coupler. (b) Coupling loss versus different tip widths of the lower LN inversed taper (TE mode at 1550 nm).

Couplers with various tip widths of the lower LN inversed taper were tested. The simulated and measured coupling loss at 1550 nm versus different tip widths taper were shown in Fig. 7(b). As expected, the loss rises when the tips get wider, while the loss is still as low as 0.72 dB when the tip width reaches 400 nm. This result shows the large tolerance of fabrication error and relatively low requirement of lithography resolution for the proposed coupler. The difference of the coupling loss between experiment and simulation might come from the imperfections induced in fabrication process, optical absorption of the material and the mismatching between the mode of the fiber and the fabricated coupler.

The tolerance of the alignment between the coupler and the fiber is measured through shifting the fiber from the optimum coupling position along X and Z direction, as shown in Fig. 8(a). For TE light, 1μm of misalignment between fiber and coupler along X/Z direction leads to a 0.6 dB additional loss per facet. Our coupler shows a relatively large tolerance of misalignment, which will reduce the cost of optical packaging and increase the reliability of LNOI devices in practical applications.

High optical power is necessary in some situations such as nonlinear optics applications. However, high optical power leads to degradation of coupling efficiency due to the change of refractive index induced by photo damage and photothermal effect. Figure 8(b) shows the coupling loss at different input powers. The high-power light is obtained by optical amplification using an EDFA. The loss increases by about 0.4 dB when the input power is increased to 30 dBm (1 W), while it remains lower than 1dB/facet making it promising for high power applications.

After fixing the fiber array of the UHNAF with the chip using UV curing adhesive, we study the dependence of the coupling loss on the environment temperature in the range of -45 ℃ to 75 ℃. The junction between the fiber array and the chip is shown in Fig. 9(a). And the result of thermal loop test is shown in Fig. 9(b). It shows a very low sensitivity to environment temperature. The max degradation of coupling efficient for TE light is less than 0.01 dB. The impressive result of thermal loop indicates the potential of our coupler to for industrial applications. The coupling

Optics EXPRESS

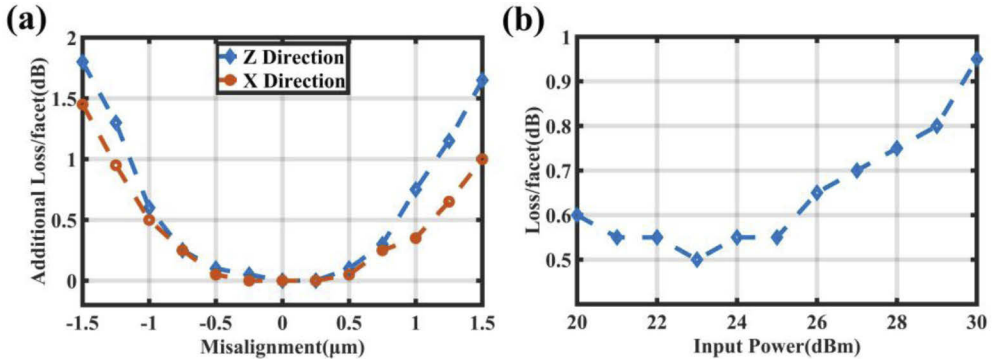

Fig. 8. (a) Dependence of additional coupling loss on fiber-chip misalignment (TE mode at 1550 nm). (b) Dependence of coupling loss on optical input power (TE mode at 1550 nm).

loss when the fiber array is affixed with the UV curable adhesive is about 1.2dB/facet for TE mode at 1550 nm. The excess loss may come from the misalignment between the fiber array and the coupler introduced by the shrink of the UV adhesive when it is curing. The excess loss can be decrease by optimize the packaging technology in the future. The refractive index of the adhesive is about 1.56.

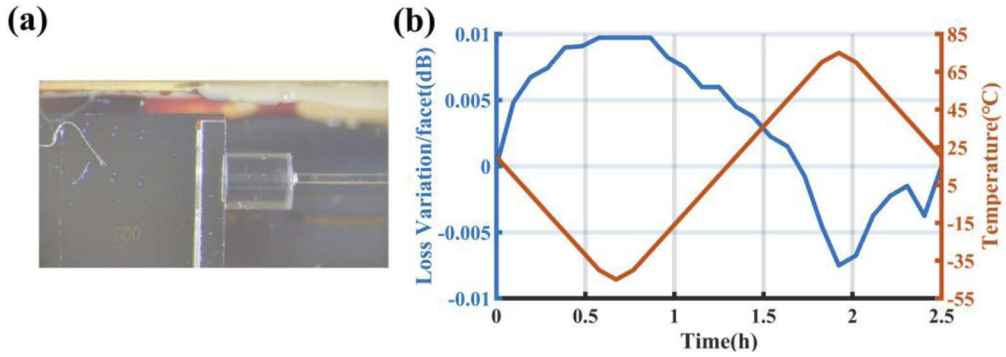

Fig. 9. (a) The junction between fiber array for UHNAF and the chip. (b) The dependence of coupling loss on environment temperature (TE mode at 1550 nm).

4. Conclusion

In this paper, we demonstrated an edge coupler for LNOI devices through combining a bilayer inversed taper and a CLDWG. The proposed coupler shows high efficiency, polarization independence and high stability. The coupler is fabricated by standard semiconductor process, making it possible for massive production at low cost. A low coupling loss of 0.54 dB/0.59 dB per facet for TE/TM light is achieved. The coupling loss is lower than 1dB/facet for both TE and TM light in the wavelength range of 1527 nm to 1630 nm. A relatively large tolerance for optical misalignment is also proved. The coupler shows a promising stability in high optical power and temperature variation. The demonstrated edge coupler will push LNOI devices closer to practical applications.

Funding. National Key Research and Development Program of China (2019YFB2203501); National Natural Science Foundation of China (61835008, 61905079, 61905084); State Key Laboratory of Advanced Optical Communication Systems and Networks. (2019GZKF03008).

Optics EXPRESS

Acknowledgments. We thank the Center of Micro-Fabrication and Characterization (CMFC) of WNLO and the Center for Nanoscale Characterization & Devices (CNCD), WNLO of HUST for the facility support.

Disclosures. The authors declare no conflicts of interest.

Supplemental document. See Supplement 1 for supporting content.

References

1. F. Kish, V. Lal, P. Evans, S. W. Corzine, M. Ziari, T. Butrie, M. Reffle, H.-S. Tsai, A. Dentai, J. Pleumeekers, M. Missey, M. Fisher, S. Murthy, R. Salvatore, P. Samra, S. Demars, N. Kim, A. James, A. Hosseini, P. Studenkov, M. Lauermann, R. Going, M. Lu, J. Zhang, J. Tang, J. Bostak, T. Vallaitis, M. Kuntz, D. Pavinski, A. Karanicolas, B. Behnia, D. Engel, O. Khayam, N. Modi, M. R. Chitgarha, P. Mertz, W. Ko, R. Maher, J. Osenbach, J. T. Rahn, H. Sun, K.-T. Wu, M. Mitchell, and D. Welch, "System-on-Chip Photonic Integrated Circuits," IEEE J. Sel. Top. Quantum Electron. **24**(1), 1–20 (2018).
2. V. Lal, J. Summers, N. Kim, S. W. Corzine, P. Evans, M. Lauermann, A. Nguyen, A. Hosseini, M. Lu, J. T. Rahn, M. R. Chitgarha, J. Zhang, J. Osenbach, T. Vallaitis, P. Samra, C. Park, M. Kuntz, J. Tang, C. Tsai, H. Sun, R. Schmogrow, D. Pavinski, B. Behnia, P. Mertz, T. Butrie, K.-T. Wu, M. Mitchell, M. Ziari, M. Reffle, D. Welch, and F. Kish, "Extended C-Band Tunable Multi-Channel InP-Based Coherent Transmitter PICs," J. Lightwave Technol. **35**(7), 1320–1327 (2017).
3. A. Pan, C. Hu, C. Zeng, C. Zeng, J. Xia, and J. Xia, "Fundamental mode hybridization in a thin film lithium niobate ridge waveguide," Opt. Express **27**(24), 35659–35669 (2019).
4. Y. Yao, H. Liu, L. Xue, B. Liu, and H. Zhang, "Design of lithium niobate phase-shifted Bragg grating for electro-optically tunable ultra-narrow bandwidth filtering," Appl. Opt. **58**(25), 6770–6774 (2019).
5. C. Wang, M. Zhang, X. Chen, M. Bertrand, A. Shams-Ansari, S. Chandrasekhar, P. Winzer, and M. Lončar, "Integrated lithium niobate electro-optic modulators operating at CMOS-compatible voltages," Nature **562**(7725), 101–104 (2018).
6. C. Wang, M. Zhang, M. Yu, R. Zhu, H. Hu, and M. Loncar, "Monolithic lithium niobate photonic circuits for Kerr frequency comb generation and modulation," Nat. Commun. **10**(1), 978 (2019).
7. R. Luo, Y. He, H. Liang, M. Li, and Q. Lin, "Highly tunable efficient second-harmonic generation in a lithium niobate nanophotonic waveguide," Optica **5**(8), 1006–1011 (2018).
8. C. Wang, C. Langrock, A. Marandi, M. Jankowski, M. Zhang, B. Desiatov, M. M. Fejer, and M. Lončar, "Ultrahigh-efficiency wavelength conversion in nanophotonic periodically poled lithium niobate waveguides," Optica **5**(11), 1438–1441 (2018).
9. D. Pohl, M. Reig Escalé, M. Madi, F. Kaufmann, P. Brotzer, A. Sergeyev, B. Guldimann, P. Giaccari, E. Alberti, U. Meier, and R. Grange, "An integrated broadband spectrometer on thin-film lithium niobate," Nat. Photonics **14**(1), 24–29 (2020).
10. V. Ramaswamy, R. C. Alferness, and M. Divino, "High efficiency single-mode fibre to Ti:LiNbO3 waveguide coupling," Electron. Lett. **18**(1), 30–31 (1982).
11. M. S. Nisar, X. Zhao, A. Pan, S. Yuan, and J. Xia, "Grating Coupler for an On-Chip Lithium Niobate Ridge Waveguide," IEEE Photonics J. **9**(1), 1–8 (2017).
12. R. Ulrich, "Theory of the Prism–Film Coupler by Plane-Wave Analysis," J. Opt. Soc. Am. **60**(10), 1337–1350 (1970).
13. N. Yao, N. Yao, J. Zhou, J. Zhou, J. Zhou, R. Gao, R. Gao, J. Lin, J. Lin, J. Lin, M. Wang, M. Wang, Y. Cheng, Y. Cheng, Y. Cheng, Y. Cheng, Y. Cheng, Y. Cheng, W. Fang, W. Fang, and L. Tong, "Efficient light coupling between an ultra-low loss lithium niobate waveguide and an adiabatically tapered single mode optical fiber," Opt. Express **28**(8), 12416–12423 (2020).
14. I. Krasnokutska, J.-L. J. Tambasco, and A. Peruzzo, "Nanostructuring of LNOI for efficient edge coupling," Opt. Express **27**(12), 16578–16585 (2019).
15. L. He, M. Zhang, A. Shams-Ansari, R. Zhu, C. Wang, and L. Marko, "Low-loss fiber-to-chip interface for lithium niobate photonic integrated circuits," Opt. Lett. **44**(9), 2314–2317 (2019).
16. J. Cardenas, C. B. Poitras, K. Luke, L.-W. Luo, P. A. Morton, and M. Lipson, "High Coupling Efficiency Etched Facet Tapers in Silicon Waveguides," IEEE Photonics Technol. Lett. **26**(23), 2380–2382 (2014).
17. A. Khilo, M. A. Popović, M. Araghchini, and F. X. Kärtner, "Efficient planar fiber-to-chip coupler based on two-stage adiabatic evolution," Opt. Express **18**(15), 15790–15806 (2010).
18. T. Wahlbrink, W. S. Tsai, M. Waldow, M. Först, J. Bolten, T. Mollenhauer, and H. Kurz, "Fabrication of high efficiency SOI taper structures," Microelectron. Eng. **86**(4-6), 1117–1119 (2009).
19. T. Shoji, T. Tsuchizawa, T. Watanabe, K. Yamada, and H. Morita, "Low loss mode size converter from 0.3 μm square Si wire waveguides to singlemode fibres," Electron. Lett. **38**(25), 1669–1670 (2002).
20. B. B. Bakir, A. V. De Gyves, R. Orobtchouk, P. Lyan, C. Porzier, A. Roman, and J.-M. Fedeli, "Low-Loss (< 1 dB) and Polarization-Insensitive Edge Fiber Couplers Fabricated on 200-mm Silicon-on-Insulator Wafers," IEEE Photonics Technol. Lett. **22**(11), 739–741 (2010).
21. L. Chen, C. R. Doerr, Y.-K. Chen, and T.-Y. Liow, "Low-Loss and Broadband Cantilever Couplers Between Standard Cleaved Fibers and High-Index-Contrast Si_3N_4 or Si Waveguides," IEEE Photonics Technol. Lett. **22**(23), 1744–1746 (2010).

Optics EXPRESS

22. Q. Fang, J. Song, X. Luo, M. Yu, G. Lo, and Y. Liu, "Mode-size converter with high coupling efficiency and broad bandwidth," Opt. Express **19**(22), 21588–21594 (2011).
23. Q. Fang, T.-Y. Liow, J. F. Song, C. W. Tan, M. B. Yu, G. Q. Lo, and D.-L. Kwong, "Suspended optical fiber-to-waveguide mode size converter for Silicon photonics," Opt. Express **18**(8), 7763–7769 (2010).
24. R. G. Hunsperger, *Integrated Optics* (Springer New York, 2009), Chap. 7.
25. P. E. Barclay, K. Srinivasan, and O. Painter, "Design of photonic crystal waveguides for evanescent coupling to optical fiber tapers and integration with high-Q cavities," J. Opt. Soc. Am. B **20**(11), 2274–2284 (2003).
26. T. G. Tiecke, K. P. Nayak, J. D. Thompson, T. Peyronel, N. P. de Leon, V. Vuletić, and M. D. Lukin, "Efficient fiber-optical interface for nanophotonic devices," Optica **2**(2), 70–75 (2015).
27. S. Khan, S. M. Buckley, J. Chiles, R. P. Mirin, S. W. Nam, and J. M. Shainline, "Low-loss, high-bandwidth fiber-to-chip coupling using capped adiabatic tapered fibers," APL Photonics **5**(5), 056101 (2020).
28. H. Gehring, M. Blaicher, W. Hartmann, P. Varytis, K. Busch, M. Wegener, and W. H. P. Pernice, "Low-loss fiber-to-chip couplers with ultrawide optical bandwidth," APL Photonics **4**(1), 010801 (2019).
29. M. Blaicher, M. Blaicher, M. R. Billah, M. R. Billah, T. Hoose, T. Hoose, P.-I. Dietrich, P.-I. Dietrich, A. Hofmann, S. Randel, W. Freude, and C. Koos, "3D-Printed Ultra-Broadband Highly Efficient Out-of-Plane Coupler for Photonic Integrated Circuits," in Conference on Lasers and Electro-Optics (Optical Society of America, 2018), Paper STh1A.1.
30. Y. Pan, S. Sun, M. Xu, M. He, S. Yu, and X. Cai, "Low fiber-to-fiber loss, large bandwidth and low drive voltage lithium niobate on insulator modulators," in Conference on Lasers and Electro-Optics, OSA Technical Digest (Optical Society of America, 2020), paper JTh2B.10.
31. K. Rhoff, P. V. Lambeck, and A. Driessen, "Design, Tolerance Analysis, and Fabrication of Silicon Oxynitride Based Planar Optical Waveguides for Communication Devices," J. Lightwave Technol. **17**(8), 1401–1407 (1999).
32. R. Germann, H. W. M. Salemink, R. Beyeler, G. L. Bona, F. Horst, I. Massarek, and B. J. Offrein, "Silicon Oxynitride Layers for Optical Waveguide Applications," J. Electrochem. Soc. **147**(6), 2237 (2000).
33. Y. Maegami, R. Takei, E. Omoda, T. Amano, M. Okano, M. Mori, T. Kamei, and Y. Sakakibara, "Spot-size converter with a SiO_2 spacer layer between tapered Si and SiON waveguides for fiber-to-chip coupling," Opt. Express **23**(16), 21287–21295 (2015).